Dyes and Pigments 94 (2012) 570–582

Contents lists available at SciVerse ScienceDirect

Dyes and Pigments

journal homepage: www.elsevier.com/locate/dyepig

1, 3, 5-Triazine-cored derivatives dyes containing triphenylamine based two-photon absorption: Synthesis, optical characterization and bioimaging

Hongping Zhou [a,*], Zheng Zheng [a], Guoyi Xu [a], Zhipeng Yu [a], Xiaofei Yang [a], Longhuai Cheng [a], Xiaohe Tian [b], Lin Kong [a], Jieying Wu [a], Yupeng Tian [a,c,d]

[a] Department of Chemistry, Anhui University, Key Laboratory of Functional Inorganic Materials Chemistry of Anhui Province, 230039 Hefei, PR China
[b] Department of Biomedical Science, University of Sheffield, Sheffield, UK
[c] State Key Laboratory of Crystal Materials, Shandong University, 250100 Jinan, PR China
[d] State Key Laboratory of Coordination Chemistry, Nanjing University, 210093 Nanjing, PR China

ARTICLE INFO

Article history:
Received 3 January 2012
Received in revised form
13 March 2012
Accepted 14 March 2012
Available online 23 March 2012

Keywords:
Triazine dyes
Triphenylamine
σ-Electron pair as a bridge
Photophysical properties
2PA cross section
Two-photon fluorescence cell imaging

ABSTRACT

A series of new one, two and three-branched two-photon absorption triazine dyes containing triphenylamine with a π-bond and a σ-electron pair as a bridge, and different electron-donating groups, have been synthesized and their photophysical properties have been systematically investigated. These dyes showed obvious solvatochromic effects, i.e., significant bathochromic shifting of the emission spectra and larger Stokes shifts were observed in more polar solvents mainly due to intramolecular charge-transfer (ICT). The two-photon absorption (2PA) cross section values were determined by two-photon excited fluorescence (TPEF) measurements in DMF. This result further proved that a σ-electron pair as a bridge is an efficient way to transfer charge as well as a π bridge to provide a large 2PA cross section, and that their 2PA cross section values (δ) increase with increasing electron-donating strength of the end group and branch number. In addition, two-photon fluorescence cell imaging of dye **7a** in HeLa and MCF-7 cancer cells was demonstrated.

1. Introduction

The development of materials displaying large two-photon absorption (2PA) [1,2] has attracted great interest in past decades due to a variety of potential applications in photonics and optoelectronics, such as three-dimensional optical data storage, fluorescence imaging, optical limiting, up-converted lasing and microfabrication [3]. The big advantage of these materials is that excitation in the lower-energy near-IR region can lead to inherent higher-energy photophysical properties of the chromophores. It is important to prevent damage to the materials as a result of higher-energy photons. Besides, the quadratic dependence of two-photon absorption on excitation intensity causes photochemistry to occur in a small focal region, allowing for more control in microfabrication and imaging applications [4]. In the early 1990s, two-photon fluorescence (2PF) imaging was pioneered by Webb et al. [5]. Since then it has become the technique of choice for noninvasive biological imaging in thick tissue and living animals, due to the above merits it provides.

However, most of the currently used one-photon excited biological fluorophores show low 2PA cross sections (δ) and are thus limited their use in 2PF imaging. Therefore, there is a pressing need to synthesize materials with large 2PA cross sections for *in vivo* imaging. Some design strategies for the construction of molecules with large two-photon absorption cross sections (δ) have been studied from both experimental [6,7,14] and theoretical [8,9] perspectives. The accumulated knowledge and experience from many research groups to understand the connections between molecular structure and 2PA properties by testing and modeling various dye systems since the mid-1990s have revealed that molecular 2PA is related to a combination of several structural parameters, such as intramolecular charge-transfer (ICT) efficiency and/or the effective size of the π-conjugation domain within a molecule, i.e., the conjugation length and strength of the donor and acceptor [10,11]. Besides, designing a multi-branched backbone molecular structure is one of the effective strategies [11,12] to obtain a large 2PA cross section, as the branched architecture not only provides a way to incorporate several 2PA-enhancing parameters into a single system, but also allows material chemists to optimize a dye molecule by combining various desired characteristics together for specific purposes. Cho et al [13–16] reported that

* Corresponding author. Tel.: +86 551 5108151; fax: +86 551 5107342.
E-mail address: zhpzhp@263.net (H. Zhou).

0143-7208/$ – see front matter © 2012 Elsevier Ltd. All rights reserved.
doi:10.1016/j.dyepig.2012.03.017

the π-conjugated core played a major role in the branched octupolar molecules' 2PA properties, and the three-arm octupolar structure showed significant improvement of the 2PA response in comparison with singly or doubly branched counterparts [17,18].

On the other hand, the fluorescence quantum yields of a majority of 2PA materials are found to decrease at high concentration due to the aggregation of molecules, which generally leads to fluorescence quenching in the solid state. Consequently a special molecular design for a 2PA material is required not only to ensure a large two-photon activity, but more importantly, to overcome fluorescence quenching at high concentration. Very recently, Tian et al. [19] reported two new AIE (aggregation-induced emission)-active multi-branched molecules with a 1, 3, 5-triazine core, which exhibit aggregation-induced emission and a large two-photon absorption cross section (8629 GM). Hua et al. [20] reported a series of new multi-branched triazine chromophores containing triphenylamine derivatives and demonstrated that multi-branched triazine chromophores are a highly suitable class of two-photon absorbing materials. To date, most of studies about the two-photon materials have been focused on employing C=C bonds as the linkage to combine a 1, 3, 5-triazine core with an electron-donating end group while very little attention has been paid to the alteration of the acceptor–donor linkage. Recently, spectral, and photophysical characteristics of some *N*-triazinyl derivatives has been reported [21], but 2PA and applications of such materials are studied rarely. Wang et al. [22] reported a new 2PA-active compound employing a nitrogen atom as the linkage to combine a 1, 3, 5-triazine core with substituents. This new strategy can not only increase the solubility in common organic solutions, but can also offer the advantages of increasing internal rotation of the chromophores in the monomer form without causing aggregation in media, and electron delocalization is favoured. Based on that, we were motivated to design a series of dyes containing a 1, 3, 5-triazine unit and investigate their structure–property relationships as 2PA materials.

On the basis of these interesting findings, we intend to connect two electron-donating groups diphenyl and diethoxyphenyl to one nitrogen of 1, 2-bis(4-aminophenyl)ethylene, which is connected to the electron-withdrawing 1, 3, 5-triazine core through a σ-electron pair on the N atom, to build up new octupolar 2PA dyes. This idea is also based on the following considerations: (1) 1, 3, 5-triazine-based compounds show good optical and electrical properties due to high electron affinity and symmetrical structure [23]. In particular, octupolar molecules consisting of a strong triazine electron-accepting center and an electron-donating end group linked through a π-conjugated bridge have proved to be excellent 2PA materials, because of high coplanarity of the conjugated system, strong intramolecular charge-transfer (ICT), and additional cooperative enhancement between the branches [24]. (2) Triphenylamine has been widely used in opto- and electroactive materials, due to their good electron-donating and transporting capabilities, as well as their special propeller starburst molecular structure [25]. (3) A σ-electron pair as a bridge can be used to not only extend the molecular conjugated system and promote solubility, but also to avoid the aggregation-induced fluorescence quenching of the strong π–π stacking interaction in these large flat π-systems.

Here we have strategically designed and presented a similar one-step method to prepare of a series of new pull-push type octupolar triazine dyes (**7a**–**7b**) and their one-and two-branched dyes (**5a**–**5b, 6a**–**6b**) by changing the ratio of RNH_2 and 2, 4, 6-trichloro-1, 3, 5-triazine, upon incorporating different electron-donating groups with 1, 3, 5-triazine. Linear photophysical characterization and investigation of 2PA properties are presented as a basis for potential applications in two-photon fluorescence imaging.

2. Experimental section

2.1. Materials and physical measurements

IR spectra were recorded with a Nicolet FT-IR NEXUS 870 spectrometer (KBr discs) in the 4000–400 cm^{-1} region. ^1H and ^{13}C NMR spectra were recorded on a 400 or 500 MHz NMR instrument using $CDCl_3$ or $(CD_3)_2CO$ as solvent. Chemical shifts were reported in parts per million (ppm) relative to internal TMS (0 ppm) and coupling constants in Hz. Splitting patterns were described as singlet (s), doublet (d), triplet (t), quartet (q), or multiplet (m). Mass spectra were obtained on a Micromass GCT-MS Spectrometer. MALDI-TOF mass spectra were recorded on a time-of-flight (TOF) mass spectrometer using a 337 nm nitrogen laser with alpha-cyano-4-hydroxycinnamic acid as matrix.

2.2. Optical measurements

The one-photon absorption (OPA) spectra were recorded on a UV-265 spectrophotometer. The one-photon excited fluorescence (OPEF) spectra measurements were performed using a Hitachi F-7000 fluorescence spectrophotometer. OPA and OPEF of dyes **5a**–**7a**, **5b**–**7b** were measured in five organic solvents of different polarities with the concentration of 1.0×10^{-5} mol L^{-1}. The quartz cuvettes used are of 1 cm path length. The fluorescence quantum yields (Φ) were determined by using coumarin 307 as the reference according to the literature method [26]. Quantum yields were corrected as follows:

$$\Phi_s = \Phi_r \left(\frac{A_r \eta_s^2 D_s}{A_s \eta_r^2 D_r} \right)$$

where the *s* and *r* indices designate the sample and reference samples, respectively, *A* is the absorbance at λ_{exc}, η is the average refractive index of the appropriate solution, and *D* is the integrated area under the corrected emission spectrum [27].

Two-photon absorption (2PA) cross sections (δ) of the samples were obtained by two-photon excited fluorescence (TPEF) method [28] at femtosecond laser pulse and Ti: sapphire system (680–1080 nm, 80 MHz, 140 fs) as the light source. The sample was dissolved in different solvents at a concentration of 1.0×10^{-3} mol L^{-1}. The intensities of TPEF spectra of the reference and the sample were determined at their excitation wavelength. Thus, 2PA cross section (δ) of samples was determined by Eq.:

$$\delta = \delta_{ref} \frac{\Phi_{ref}}{\Phi} \frac{c_{ref}}{c} \frac{n_{ref}}{n} \frac{F}{F_{ref}}$$

Where the ref subscripts stand for the reference molecule (here coumarin 307 in ethanol solution at concentration of 1.0×10^{-3} mol L^{-1} was used as reference). δ is the 2PA cross-sectional value, *c* is the concentration of the solution, *n* is the refractive index of the solution, *F* is the TPEF integral intensities of the solution emitted at the exciting wavelength, and Φ is the fluorescence quantum yield. The δ_{ref} value of reference was taken from the literature [29].

2.3. Materials and synthesis

Triphenylamine, 4-iodophenol, and cyanuric chloride were available commercially, and the solvents were purified as conventional methods before use. These compounds were characterized by ^1H NMR, ^{13}C NMR, FT-IR, and MS spectrometry.

2.3.1. Preparation of *3a*

0.6 g (5.4 mmol) *t*-BuOK was placed into a dry mortar and well milled into powder, then 1.0 g (2.2 mmol) **1** and 0.5 g (1.8 mmol) **2a**

were added and mixed. The mixture was milled vigorously and monitored by TLC. The mixture became sticky and was continuously milled for another 10 min. After completion of the reaction, the mixture was dissolved in 100 mL CH_2Cl_2. The mixture was filtered and concentrated. The product was recrystallized from anhydrous ethanol, to give 0.33 g red arborescent solid. Yield: 47.0%. ^{1}H NMR: (400 Hz, $(CD_3)_2CO$), δ (ppm): 8.23 (d, J = 8.0 Hz, 2H), 7.85 (d, J = 8.4 Hz, 2H), 7.60 (d, J = 8.0 Hz, 2H), 7.51 (d, J = 16.4 Hz, 1H), 7.35 (d, J = 7.8 Hz, 4H), 7.38 (d, J = 16.4, 1H), 7.13 (d, J = 7.2 Hz, 6H), 7.03 (d, J = 8.0 Hz, 2H). ^{13}C NMR (125 MHz, $CDCl_3$): δ (ppm) = 148.7, 147.8, 147.4, 146.5, 145.0, 144.5, 133.5, 133.0, 130.0, 129.7, 129.5, 129.4, 128.2, 126.7, 126.5, 125.1, 124.8, 124.3, 123.8, 123.6, 122.8, 122.3. IR (KBr, cm^{-1}): 3055, 1680, 1588,1511, 1484, 1439, 1334, 1311, 995, 860, 753, 696. HRMS (GCT-MS) Calcd for $C_{26}H_{20}N_2O_2$, 392.15; Found, 392.1487.

2.3.2. Preparation of ***3b***

Black oil **3b** was obtained using **2b** instead of **2a**, with only one silica gel column chromatography step with petroleum b.p. 60–90 °C/ethyl acetate (20:1 by volume). Yield: 51.0%. ^{1}H NMR: (400 Hz, $(CD_3)_2SO$), δ (ppm): 8.19 (d, J = 8.8 Hz, 2H), 7.78 (d, J = 8.8 Hz, 2H), 7.47 (d, J = 8.4 Hz, 2H), 7.04 (t, 5H), 6.91 (t, 5H), 6.74 (d, J = 8.80 Hz, 2H), 4.00 (q, J = 7.1 Hz, 4H), 1.32 (t, J = 6.9 Hz, 6H). ^{13}C NMR (100 MHz, $CDCl_3$): δ (ppm) = 155.7, 149.5, 146.2, 144.6, 140.1, 133.2, 127.9, 127.8, 127.1, 126.3, 124.2, 123.1, 119.5, 115.4, 63.7, 14.9. IR (KBr, cm^{-1}): 2978, 2924, 1580, 1504, 1476, 1391, 1334, 1239, 954, 834. HRMS (GCT-MS) Calcd for $C_{30}H_{28}N_2O_4$, 480.20; Found, 480.2026.

2.3.3. Preparation of ***4a***

A solution of 3.0 g (10 mmol) of **3a** dissolved in 150 mL ethanol was added into a round-bottom flask equipped with a magnetic stirrer and heated at 80 °C. Then 0.3 g of Pd/C catalyst was added into the preceding reaction system and a solution of 4.9 mL of 85% hydrazine hydrate was added dropwise for about 0.5 h. The reaction was monitored by TLC. After the completion of the reaction, the reaction mixture was filtered immediately and the solution was cooled to room temperature to give a cream solid. 2.56 g of **4b** was obtained after filtration and drying in vacuo.Yield: 75.0%. ^{1}H NMR: (400 Hz, $(CD_3)_2CO$), δ (ppm): 7.45 (d, J = 8.8 Hz, 2H), 7.30 (m, 6H), 7.05 (m, 10H), 6.93 (d, J = 16.4 Hz, 1H), 6.68 (d, J = 8.4 Hz, 2H), 4.78 (s, 2H). ^{13}C NMR (100 MHz, $CDCl_3$): δ (ppm) = 147.54, 147.50, 147.3, 134.2, 131.3, 129.3, 127.6, 127.5, 127.3, 126.0, 124.5, 123.5, 123.0, 120.1. IR (KBr, cm^{-1}): 3449, 3371, 3023, 1616, 1586, 1515, 1489, 1330, 965, 834, 750, 697. HRMS (GCT-MS) Calcd for $C_{26}H_{22}N_2$, 362.18; Found, 362.1777.

2.3.4. Preparation of ***4b***

A solution of 1.09 g (2.27 mmol) of **3b** dissolved in 25 mL of ethanol was added into a round-bottom flask equipped with a magnetic stirrer and heated at 80 °C. Then 0.12 g of Pd/C catalyst was added into the preceding reaction system and a solution of 1.1 mL of 85% hydrazine hydrate dissolved in 25 mL ethanol was added dropwise for 0.5 h. The reaction was monitored by TLC. After the completion of the reaction, the solvent was removed under reduced pressure. The mixture was washed with water and extracted with ethyl acetate. The organic phase was dried over $MgSO_4$, filtered and concentrated to provide light red oil. Purification was carried out by silica gel column chromatography using petroleum (b.p. 60–90 °C)/ethyl acetate (10:1 by volume) to afford 0.61 g of yellow powder. Yield: 60.0%. ^{1}H NMR(cis-): (400 Hz, $(CD_3)_2SO$), δ (ppm): 7.10 (d, J = 8.4, 2H), 6.98 (t, J = 7.0 Hz, 6H), 6.88 (d, J = 8.8 Hz, 4H), 6.63 (d, J = 8.4 Hz, 2H), 6.44 (d, J = 8.0 Hz, 2H), 6.28 (d, J = 12.4 Hz, 1H), 6.19 (d, J = 12.4, 1H), 5.18 (s, 1H), 3.99 (q, J = 6.9 Hz, 4H), δ (ppm): 1.31 (t, J = 7.0 Hz, 6H); ^{1}H NMR(trans-): (400 Hz, $(CD_3)_2SO$), δ (ppm): 7.31 (d, J = 8.0 Hz, 2H), 7.22 (d, J = 8.0 Hz, 2H), 6.98 (d, J = 8.8 Hz, 4H), 6.86 (t, 5H), 6.78 (d, J = 16.8 Hz, 1H), 6.74 (d, J = 8.0 Hz, 2H), 6.55 (d, J = 8.4 Hz, 2H), 5.24 (s, 2H), 3.99 (q, J = 6.9 Hz, 4H), 1.32 (t, J = 6.8 Hz, 6H). ^{13}C NMR (125 MHz, $CDCl_3$): δ (ppm) = 155.3, 148.0, 143.3, 140.9, 140.8, 130.2, 127.5, 127.2, 127.0, 126.6, 126.0, 125.8, 125.5, 120.9, 120.7, 120.5, 116.7, 115.4, 63.8, 15.1. IR (KBr, cm^{-1}): 3452, 3374, 3028, 2979, 2925, 1607, 1503, 1476, 1392, 1283, 1238, 1046, 962, 827. HRMS (GCT-MS) Calcd for $C_{30}H_{30}N_2O_2$, 450.23; Found, 450.2336.

2.3.5. Preparation of ***5a***

A suspension of 1.0 g (5.5 mmol) of cyanuric chloride, 4.8 mL of N, N-Diisopropylethylamine (DIPEA) dissolved in 20 mL of dry THF was added into a round-bottom flask equipped with a magnetic stirrer in an ice-salt bath, and a solution of 2 g (5.5 mmol) of **4a** dissolved in 10 mL dry THF was added dropwise with stirring for 1 h. The reaction was monitored by TLC. After the completion of the reaction, the solvent was removed under reduced pressure and the residue was purified by column chromatography with petroleum (b.p. 60-90 °C)/ethyl acetate (20:1 by volume) to give 1.2 g of yellow solid. Yield: 43.0%. ^{1}H NMR: (400 Hz, $(CD_3)_2CO$), δ (ppm): 9.89 (s, 1H), 7.68 (d, J = 8.4 Hz, 2H), 7.38 (d, J = 8.4 Hz, 2H), 7.31 (t, J = 7.8 Hz, 4H), 7.22 (d, J = 8.8 Hz, 2H), 7.07 (q, J = 6.3 Hz, 6H), 6.91 (d, J = 8.8 Hz, 2H), 6.61 (d, J = 12.0 Hz, 1H), 6.57 (d, J = 12.0 Hz, 1H). ^{13}C NMR (125 MHz, $CO(CD_3)_2$): δ (ppm) = 169.6, 164.3, 147.6, 147.4, 136.1, 134.8, 131.7, 129.4, 127.9, 127.5, 126.8, 126.2, 124.4, 123.3, 123.2, 121.6. IR (KBr, cm^{-1}): 3285, 3028, 2924, 1591, 1555, 1510, 1492, 1388, 1280, 1228, 1168, 1021, 961, 836, 753, 696. HRMS (GCT-MS) Calcd for $C_{29}H_{21}Cl_2N_5$, 509.12; Found, 509.1193.

2.3.6. Preparation of ***5b***

A suspension of 1.0 g (5.4 mmol) of cyanuric chloride, 4.7 mL of DIPEA dissolved in 10 mL of dry THF was added into a round-bottom flask equipped with a magnetic stirrer in an ice-salt bath, and a solution of 2.42 g (5.4 mmol) of **4b** dissolved in 10 mL dry THF was added dropwise for 1 h. The reaction was monitored by TLC. After the completion of the reaction, the solvent was removed under reduced pressure and the residue was purified by column chromatography with petroleum (b.p. 60–90 °C)/ethyl acetate (20:1 by volume) to give 1.03 g of yellowish-brown solid. Yield: 32.0%. ^{1}H NMR: (400 Hz, $(CD_3)_2CO$), δ (ppm): 9.90 (s, 1H), 7.73 (d, J = 8.4 Hz, 2H), 7.61 (d, J = 8.4 Hz, 2H), 7.41 (d, J = 8.4 Hz,2H), 7.17 (d, J = 16.4 Hz, 1H), 7.06 (m, 5H), 6.90 (d, J = 8.8 Hz, 4H), 6.84 (d, J = 8.4 Hz, 2H), 4.04 (q, J = 6.8 Hz, 4H), 1.37 (t, J = 6.8 Hz, 6H). ^{13}C NMR (100 MHz, $CDCl_3$): δ (ppm) = 170.5, 165.2, 156.7, 149.5, 141.3, 136.7, 136.0, 130.3, 129.2, 128.2, 127.7, 127.5, 125.8, 122.5, 120.6, 116.2, 64.2, 15.2. IR (KBr, cm^{-1}): 3382, 2977, 2926, 1599, 1545, 1503, 1477, 1390, 1319, 1288, 1046, 1017, 961, 829, 795. HRMS (GCT-MS) Calcd for $C_{33}H_{29}Cl_2N_5O_2$, 597.17; Found, 597.1743.

2.3.7. Preparation of ***6a***

A suspension of 0.12 g (0.65 mmol) of cyanuric chloride, 1.2 mL of DIPEA, 0.25 g (0.65 mmol) of **4a** and 10 mL of dry THF was added into a round-bottom flask equipped with a magnetic stirrer .The mixture was stirred at room temperature for 4 h and refluxed at 70 °C for 8 h. Another molar amount of **4a** (0.25 g, 0.65 mmol) was added into the preceding reaction system. The reaction was refluxed and monitored by TLC. After the completion of the reaction, appropriate amount of CH_2Cl_2 was added and the solution was washed with water. The organic phase was dried with anhydrous $MgSO_4$, filtered, concentrated and recrystallized with ethanol to give 0.17 g of yellow solid. Yield: 52.7%. ^{1}H NMR: (400 Hz, $(CD_3)_2SO$), δ (ppm): 9.93 (s, 1H), 7.64 (d, J = 8.0 Hz, 2H), 7.52 (d, J = 8.0 Hz, 2H), 7.32 (t, J = 7.4 Hz, 4H), 7.22 (d, J = 16.4 Hz, 1H), 7.15 (d, J = 16.4 Hz, 1H), 7.08 (t, J = 8.8 Hz, 6H), 7.01 (d, J = 8.0 Hz, 2H). ^{13}C

NMR (125 MHz, $CDCl_3$): δ (ppm) = 168.4, 164.1, 148.3, 136.6, 135.2, 132.1, 130.1, 128.7, 128.1, 127.5, 126.8, 125.2, 124.2, 123.8, 122.2. IR (KBr, cm^{-1}): 3385, 3025, 1591, 1570, 1493, 1414, 1278, 1075, 961, 831, 753, 695. MALDI-TOF Calcd for $C_{55}H_{42}ClN_7$, 835.32; Found, 836.1.

*2.3.8. Preparation of **6b***

A suspension of 0.61 g (3.33 mmol) of cyanuric chloride, 2.9 mL of N,N-Diisopropylethylamine, 1.5 g (3.33 mmol) of **4b** and 25 mL of dry THF was added into a round-bottom flask equipped with a magnetic stirrer .The mixture was stirred at room temperature for 4 h. Another molar amount of **4b** (1.5 g, 3.33 mmol) was added into the preceding reaction system. Then the reaction mixture was refluxed at 70 °C for 8 h and monitored by TLC. After the completion of the reaction, appropriate amount of ethanol was added with stirring and the solution was filtered to give a yellow solid. The residue was purified by column chromatography with petroleum (b.p. 60–90 °C)/ethyl acetate (6:1 by volume) to give 1.7 g of yellow solid. Yield: 51.4%. ^{1}H NMR: (400 Hz, $(CD_3)_2SO$), δ (ppm): 10.33 (s, 1H), 7.62 (d, J = 8.4 Hz, 2H), 7.51 (d, J = 8.0 Hz, 2H), 7.37 (d, J = 7.2 Hz, 2H), 7.13 (d, J = 16.4 Hz, 1H), 7.00 (m, 5H), 6.89 (d, J = 8.4 Hz, 4H), 6.74 (d, J = 7.6 Hz, 2H), 3.99 (q, J = 6.7 Hz, 4H), 1.32 (t, J = 7.0 Hz, 6H). ^{13}C NMR (125 MHz, $CDCl_3$): δ (ppm) = 169.1, 164.9, 156.2, 148.9, 140.9, 138.4, 134.2, 130.6, 130.2, 129.7, 128.4, 127.8, 127.5, 127.0, 126.3, 122.5, 120.4, 116.5, 64.3, 15.9. IR (KBr, cm^{-1}): 3383, 3028, 2976, 2925, 1599, 1559, 1503, 1413, 1391, 1237, 1045, 827, 723. MALDI-TOF Calcd for $C_{63}H_{58}ClN_7O_4$, 1011.42; Found, 1011.7.

*2.3.9. Preparation of **7a***

A suspension of 0.35 g (1.9 mmol) of cyanuric chloride, 2.08 g (5.7 mmol) of intermediate **4a**, 1.6 mL of DIPEA and 10 mL of THF under nitrogen was added into a three-necked flask equipped with a magnetic stirrer, a reflux condenser, and a nitrogen input tube. The mixture was heated to 70 °C and 1.0 g (9.5 mmol) of Na_2CO_3 and 5 mL of DMF were added. The reaction was heated to 140 °C after 30 min and then 0.06 g (5 mol %) $Pd(PPh_3)_4$ was added into the flask. The reaction mixture was refluxed under nitrogen about 30 h and monitored by TLC. Then appropriate amount of CH_2Cl_2 was added and the solution was washed with water. The organic phase was dried with anhydrous $MgSO_4$, filtered and concentrated. The yellow product was purified by column chromatography with petroleum b.p. 60–90 °C/ethyl acetate (8:1 by volume) as eluent to yield 0.89 g of yellow solid. Yield:41.2%. ^{1}H NMR: (400 Hz, $(CD_3)_2SO$), δ (ppm): 9.40 (s, 1H), 7.83 (s, 4H), 7.51 (t, J = 7.8 Hz, 8H), 7.32 (t, J = 8.2 Hz, 8H), 7.7 (m, 16H), 6.96 (d, J = 8.4 Hz, 4H). ^{13}C NMR (125 MHz, $CDCl_3$): δ (ppm) = 163.5, 148.2, 147.6, 132.8, 130.8, 128.6, 128.4, 128.1, 127.7, 127.1, 126.6, 125.2, 125.0, 124.3, 121.9, 120.8. IR (KBr, cm^{-1}): 3393, 3025, 1685, 1590, 1513, 1489, 1414, 1279, 1075, 961, 833, 753, 696. MALDI-TOF Calcd for $C_{81}H_{63}N_9$, 1161.52; Found, 1162.3.

*2.3.10. Preparation of **7b***

A suspension of 0.12 g (0.66 mmol) of cyanuric chloride, 1.2 mL of DIPEA, 0.89 g (1.98 mmol) of **4b** and 10 mL of THF under nitrogen was added into a three-necked flask equipped with a magnetic stirrer, a reflux condenser, and a nitrogen input tube. The mixture was heated to 70 °C and 0.7 g (9.5 mmol) of Na_2CO_3 and 10 mL of DMF were added. The reaction was heated to 140 °C after 30 min and then a catalytic amount of $Pd(PPh_3)_4$ was added into the flask. The reaction mixture was refluxed under nitrogen about 30 h and monitored by TLC. Appropriate amount of ethyl acetate was added and the solution was washed with water. The organic phase was dried with anhydrous $MgSO_4$, filtered and concentrated. The crude product was purified by column chromatography with petroleum (b.p. 60–90 °C)/ethyl acetate (10:1 by volume) as eluent to yield 0.21 g of yellow solid. Yield: 22.7%. ^{1}H NMR: (400 Hz, $(CD_3)_2SO$), δ (ppm): 9.30 (s, 2H), 7.75 (d, J = 5.2 Hz, 4H), 7.44 (d, J = 8.0 Hz, 4H), 7.34 (d, J = 8.0 Hz, 4H), 6.95 (d, J = 8.4 Hz, 12H), 6.85 (d, J = 8.4 Hz, 8H), 6.71 (d, J = 8.0 Hz, 4H), 3.95 (q, J = 6.7 Hz, 8H), 1.28 (t, J = 6.8 Hz, 12H). ^{13}C NMR (125 MHz, $CDCl_3$): δ (ppm) = 165.1, 156.2, 148.8, 141.0, 140.2, 132.5, 130.5, 128.3, 127.8, 127.4, 126.7, 121.5, 120.5, 116.5, 64.3, 15.9. IR (KBr, cm^{-1}): 3397, 3026, 2977, 2925, 1599, 1569, 1504, 1413, 1317, 1238, 1046, 961, 828. MALDI-TOF Calcd for $C_{93}H_{87}N_9O_6$, 1425.68; Found, 1426.17.

2.3.11. Cell culture and incubation

MCF-7 (human breast cancer cell line) cells were seed and plated on a T75 Flask and cultured in RPMI-1640 Media (Sigma–Aldrich) supplemented with 10% fetal bovine serum (Sigma), 1% L-glutamine, 1% penicillin, and 1% streptomycin, at 37 °C in a humid atmosphere with 5% CO_2 and 95% air for 2 h incubation, and then MCF-7 cells were seeded in BD Falcon™ Clear 96-well Microtest™ Plate at a density of 1×10^4 cells per well and incubated at the same conditions as indicated above until 80–90% confluency was reached. Stock solutions of dye **7a** dissolved in DMSO were prepared at concentrations of 1 μM in PBS. For live cell imaging, cell cultures were incubated with complex dye **7a** solution at and maintained at 37 °C in an atmosphere of 5% CO_2 and 95% air for 2 h incubation. The cells were washed with PBS buffer (2×200 ul per well). Costaining was performed using 2 μM SYTO9® (λ_{ex} = 488, λ_{em} = 500–530 nm) and 10 μM PI (λ_{ex} = 543, λ_{em} = 560–580 nm) for 10 min in PBS then cells were washed with PBS buffer (2×200 ul per well) and 200 ul of PBS was added to each well, and the cells were taken to a two-photon microscope for imaging without fixation.

2.3.12. Two-photon fluorescence imaging

The cells were imaged in a tissue culture chamber (5% CO_2, 37 °C) and through a Zeiss 510 LSM (upright configuration) confocal microscope with a femtosecond-pulsed Ti:Sapphire laser. The excitation beam produced by the fs laser, was tunable from 720 to 900 nm, (λ_{ex} = 720 nm, ~1 mW), which was passed through an LSM 510 microscope with HFT 650 dichroic and focused onto the cover-slip adherent cells using a 40× water immersion objective.

2.3.13. Cytotoxicity tests [MTT (3-(4,5-dimethylthiazol-2-yl)-2,5-tetrazolium bromide) assays]

To ascertain the cytotoxic effect of dyes **6a**–**7a**, **6b**–**7b** treatment over a 24 h period, the MTT assay was performed. MCF-7 cells were passed and plated to 80 %–90% confluence in 24-well plates 24 h before treatment. Prior to dyes **6a**–**7a**, **6b**–**7b** treatment, the RPMI was removed and replaced with fresh media, and then aliquots of dyes **6a**–**7a**, **6b**–**7b** stock solutions (500 μM in DMSO) were added to obtain final concentrations of 1, 5 and 10 μM. The treated cells were incubated for 24 h at 37 °C and under 5% CO_2. Subsequently, the cells were treated with 5 mg/mL MTT (1 mL/well) and incubated for an additional 1 h (37 °C, 5% CO_2). Then DMEM was removed, the cells were dissolved in DMSO (400 mL/well), and the excitation wavelengths were recorded. The cell viability (%) was calculated according to the following equation: Cell viability % $OD_{570(sample)}/OD_{570(control)} \times 100$, where $OD_{570(sample)}$ represents the optical density of the wells treated with various concentration of dyes **6a**–**7a**, **6b**–**7b** and $OD_{570(control)}$ represents that of the wells treated with DMEM + 10% FCS. Three independent trials were conducted, and the average and standard deviations are reported. The reported percent cell survival values are relative to untreated control cells.

3. Results and discussion

The targeted dyes (**5a**–**5b**, **6a**–**6b** and **7a**–**7b**) were synthesized according to Scheme 1. On the one hand, the ethyoxyl chains on the triphenylamine moieties in these model chromophores were

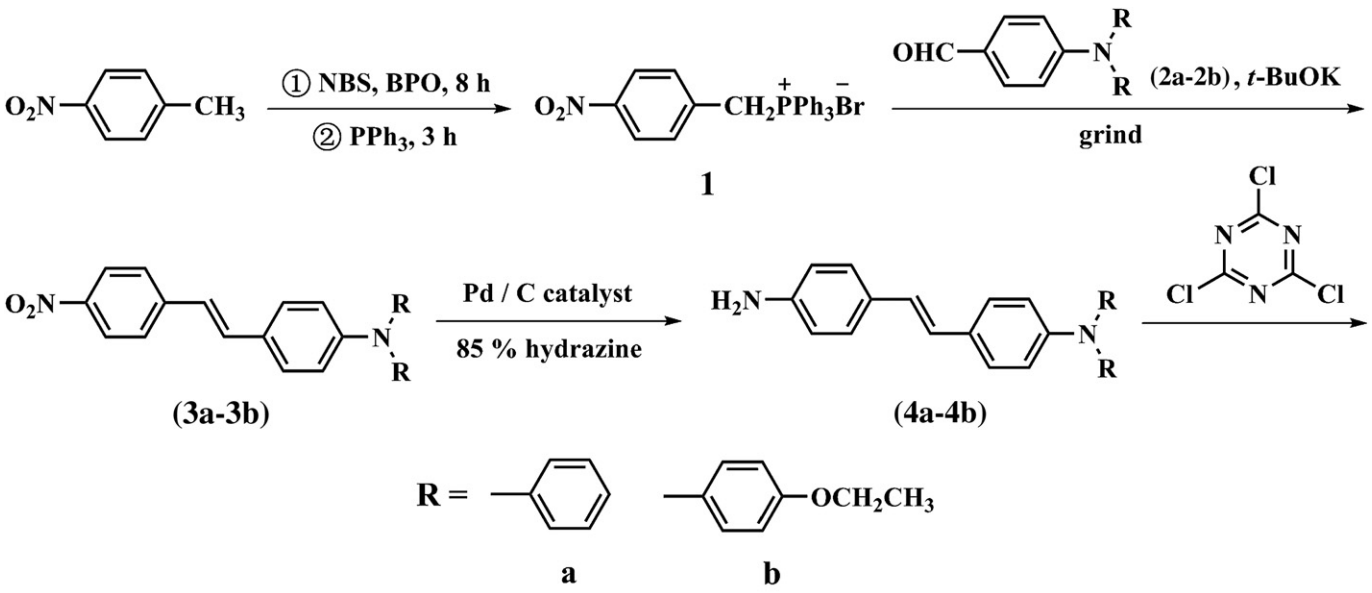

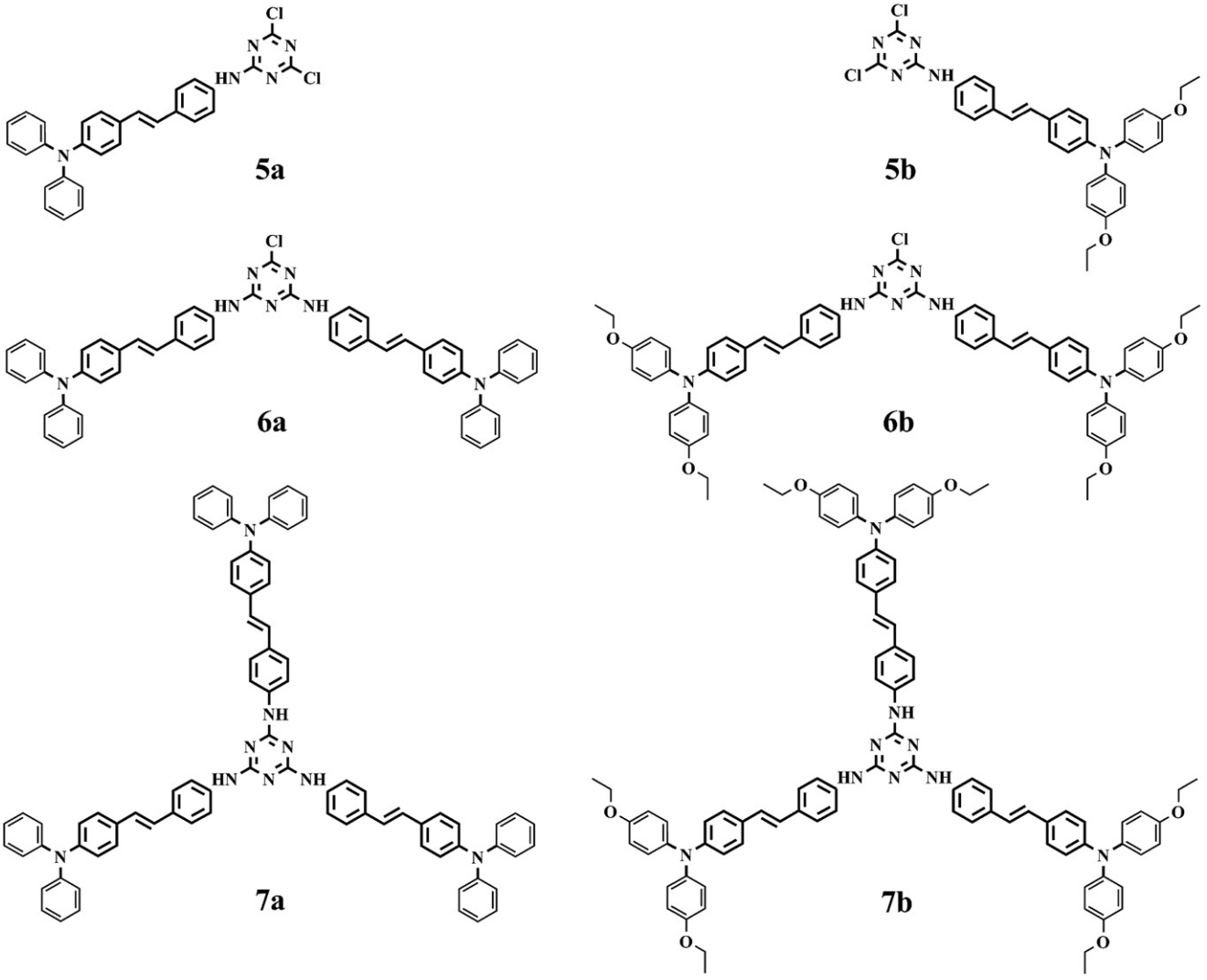

Scheme 1. Synthetic routes to target dyes **5a**–**5b**, **6a**–**6b** and **7a**–**7b**.

Table 1
The linear and Two-photon absorption properties of dyes **5a**–**5b**, **6a**–**6b** and **7a**–**7b**.

	Solvents	λ_{max}[a]	ε_{max}[b]	ε_{max}/MW[c]	λ_{max}[d]	$\Delta\nu$[e]	Φ[f]	λ_{max}[g]	σ[h]	σ/MW[i]
5a	Benzene	382	4.15		429	2868	0.071			
	THF	379	4.55		437	3502	0.132			
	Ethanol	377	4.51		437	3642	0.092			
	Acetonitrile	374	4.32		453	4663	0.056			
	DMF	**376**	**4.44 (1.0)**	**0.0087 (1.0)**	**448**	**4274**	**0.558 (5.3)**	**490**	**34**	**0.0668 (1.0)**
6a	Benzene	379	9.77		428	3021	0.310			
	THF	376	10.64		438	3765	0.294			
	Ethanol	373	10.63		442	4185	0.078			
	Acetonitrile	372	9.41		453	4807	0.114			
	DMF	**378**	**10.96(2.5)**	**0.0131 (1.5)**	**448**	**4134**	**0.134 (1.3)**	**484**	**143**	**0.1713 (2.6)**
7a	Benzene	378	10.04		429	3145	0.171			
	THF	376	11.59		439	3817	0.221			
	Ethanol	373	7.67		443	4236	0.090			
	Acetonitrile	372	5.56		453	4807	0.148			
	DMF	**377**	**11.80 (2.7)**	**0.0102 (1.2)**	**450**	**4303**	**0.106(1.0)**	**490**	**186**	**0.1601 (2.4)**
5b	Benzene	394	3.99		466	3921	0.109			
	THF	389	4.45		479	4830	0.163			
	Ethanol	386	4.14		491	5540	0.066			
	Acetonitrile	384	3.87		513	6548	0.027			
	DMF	**384**	**4.17(1.0)**	**0.0070 (1.0)**	**503**	**6161**	**0.233 (2.6)**	**530**	**103**	**0.1725 (1.0)**
6b	Benzene	388	8.08		464	4221	0.270			
	THF	386	8.97		482	5160	0.226			
	Ethanol	382	7.70		497	6057	0.104			
	Acetonitrile	383	4.54		514	6654	0.020			
	DMF	**386**	**8.24(2.0)**	**0.0081 (1.2)**	**505**	**6105**	**0.127 (1.4)**	**530**	**286**	**0.2828 (1.6)**
7b	Benzene	390	12.32		459	3855	0.178			
	THF	388	13.36		471	4542	0.152			
	Ethanol	383	12.77		491	5743	0.100			
	Acetonitrile	382	12.84		508	6493	0.067			
	DMF	**389**	**13.60 (3.3)**	**0.0095 (1.4)**	**500**	**5707**	**0.091(1.0)**	**523**	**1018**	**0.7140 (4.2)**

[a] Absorption peak position in nm (1×10^{-5} mol L^{-1}).
[b] Maximum molar absorbance in 10^4 mol^{-1} L cm^{-1}.
[c] The reduced ε_{max}, i.e. the value of ε_{max} divided by the molecular weight, the numbers in parentheses are relative values by assigning that of **5a** and **5b** as 1.
[d] Peak position of SPEF in nm (1.0×10^{-5} mol L^{-1}), excited at the absorption maximum.
[e] Stokes shift in cm^{-1}.
[f] Quantun yields determined by using coumarin 307 (1.0×10^{-5} mol L^{-1}) as the standard.
[g] TPEF peak position in nm pumped by femtosecond laser pulses at 800 mw at their maximum excitation wavelength.
[h] 2PA cross section in GM.
[i] Reduced cross section, i.e., 2PA cross section divided by molecular weight. The numbers in parentheses are relative values.

expected to enhance their solubility in common organic solvents, which is another important parameter to be considered in the molecular design of dyes for use in experimental studies and in potential. On the other hand, generally, π–π aggregation in the solid state could quench the emission of organic luminophores due to the formation of detrimental excimers, i.e., the degree of fluorescence quenching would increase with the stronger π–π stacking of the luminophores molecules. To avoid fluorescence quenching, we adopt conjugated systems of a fused σ and π-electron moieties as bridges to replace the π-conjugated bridge.

3.1. Synthesis

Synthetic routes of these series of dyes **5a**–**5b**, **6a**–**6b** and **7a**–**7b** and their intermediates are depicted in Scheme 1. The intermediate **1**, aldehyde **2a** and **2b** were synthesized efficiently according to the literature [30,31]. The yield of **2a** was 92%, while it is 40% for **2b**. Similarly, **3a** and **3b** were produced by the Wittig reaction between the Wittig reagent and the corresponding aldehyde in the solid phase with t-BuOK as base. **4a** and **4b** were prepared by the hydrazine hydrate reduction method in the presence of Pd/C catalyst in ethanol medium. The targeted dyes (**5a**–**5b**, **6a**–**6b** and **7a**–**7b**) were obtained by the palladium-catalyzed C–N coupling strategy.

3.2. One-photon absorption and emission properties

The photophysical data of dyes **5a**–**5b**, **6a**–**6b** and **7a**–**7b** are listed in Table 1. The one-photon absorption (OPA) and one-photon excited fluorescence (OPEF) were measured in five solvents of different polarities at a concentration $c = 1 \times 10^{-5}$ mol L^{-1}. To further investigate the spectra relationship of the compounds, the one-photon absorption and the one-photon excited fluorescence data of dyes **5a**–**5b**, **6a**–**6b** and **7a**–**7b** are restricted to DMF. Representative spectra of dye **7b** are shown in Fig. 1, while the others are included in the Supporting Information (Fig. S1).

3.2.1. The linear optical properties of dyes *5a–5b, 6a–6b, 7a–7b* in various solvents

As shown in Fig. 1 and Fig. S1, dyes **5a**–**5b**, **6a**–**6b** and **7a**–**7b** exhibit two major absorption bands: the peak at about 305 nm is attributed to the absorption of the triphenylamine moiety and remains almost unchanged for all the one-, two-, and three-branched dyes, while the other peak at about 372–394 nm, indicating considerable charge-transfer character. Upon increasing the solvent polarity, an obvious blue shift in absorption of dyes **5a**–**5b**, **6a**–**6b** and **7a**–**7b** was observed while the OPEF peak position λ_{max} showed an increasing tendency for the six dyes as the solvent polarity increased following the order: benzene < THF < ethanol < acetonitrile, except in DMF. There may be great changes in the molecular geometry of the excited states before fluorescence emission. The fluorescence deviation in solution can be attributed to the interaction of the solute with the local molecular environment including solvent molecules and other surrounding solute molecules. The Stokes shift also showed monotonically increasing tendency with the increase of solvent polarity except in DMF. One can see that the quantum yields (Φ) of

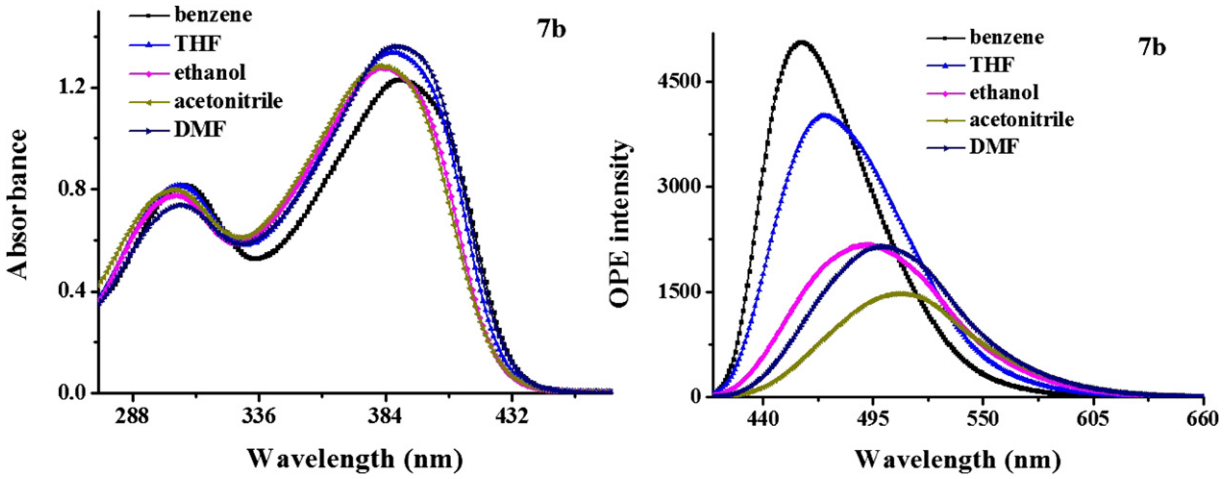

Fig. 1. Linear absorption and fluorescence of dye **7b** in five organic solvents of different polarities with a concentration of 1×10^{-5} mol L^{-1}.

dyes **6b**–**7b** decreased consistently and significantly as the polarity of solvent increases except in DMF, and were especially highly quenched in acetonitrile (Fig. 1 and Fig. S1). These can be explained by the stronger solute/solvent interaction at the excited state comparing with that at the ground state, which indicates that the increasing polarity of the excited state increases. The energy level can be lowered greatly by increasing dipole–dipole interaction between the solute and solvent. These photophysical data indicate that dyes can exhibit ICT phenomena between the fluorophore center and the amino or ethoxylated group.

3.2.2. The linear optical properties of different branches

As listed in Table 1 and Fig. 2, from dye **5b** to dye **7b** (**5a**–**7a**), the one-photon absorption maxima in DMF show regular red shifts as the branch number increases and the spectral intensities also vary regularly, the absorption coefficients (ε_{max}) of the maxima increase consistently and significantly as the branch number increases. Note that the ε_{max} of dyes **5a**–**7a** and **5b**–**7b** are of the order of 10^4 and they increase in the ratios 1.0:2.5:2.7, 1.0:2.0:3.3 with the number of chromophores. These can be assigned to the extended π-delocalization and a certain coupling between the branches in dyes **6a**, **7a** and **6b**, **7b**. The enhancement can be more clearly seen by revealing the reduced molar absorbance ε_{max}/MW which is defined as ε_{max} divided by the molecular weight. The ε_{max}/MW values increase with a ratio of 1.0:1.5:1.2 for dyes **5a**–**7a** and 1.0:1.2:1.4 for dyes **5b**–**7b**. This means that the unit molecular weight leads to larger ε_{max} by incorporating more branches into the central triazine ring.

The OPEF maxima were obtained at their maxima excitation wavelengths in DMF. From dye **5a** to dye **7a**, OPEF spectra show regular red shifts as the branch number increases (see Fig. 2). These red shifts may be ascribed to charge redistribution and extended delocalization. However, as indicated by Table 1, Fig. 2, a slight red shift in OPEF spectra is apparent in comparing dye **5b** to dye **6b**, while it is found to be obviously blue-shifted for dye **7b** relative to dyes **5b** and **6b**, respectively. It is interesting that the Stokes shift of each system shows the same increasing tendency with the OPEF as the branch number increases. This may be due to the electron-donating ability of 4-ethoxy-*N*-(4-ethoxyphenyl)-*N*-phenylaniline is higher than triphenylamine. Besides, the ICT effect should be taken into account considering the existence of an electron acceptor and chromophore served by 1, 3, 5-triazine and styryl, respectively, including the above-mentioned electron donors. The ICT state of molecules with D-π-A structures has a high photoluminescence (PL) emission ability; hence, the single peak in the PL emission spectra manifests that the state responsible for the PL emission is not the localized excited state but the ICT state. Thus, the different dipole moments of the ICT state and the ground state lead to the shift in PL spectra [24c]. Note that the fluorescence quantum yields (Φ) of dyes **5a**–**7a** and **5b**–**7b** reduce with the ratios of 5.3:1.3:1.0 and 2.6:1.4:1.0, respectively, as the branch number increases. This indicates that these dyes employed the nitrogen atom as the linkage allowing internal rotation in the monomer form in organic solvents, whereby the fluorescence was reduced. This can be ascribed to the partial conjugation structure resulting from the delocalization of the lone pair electrons on nitrogen.

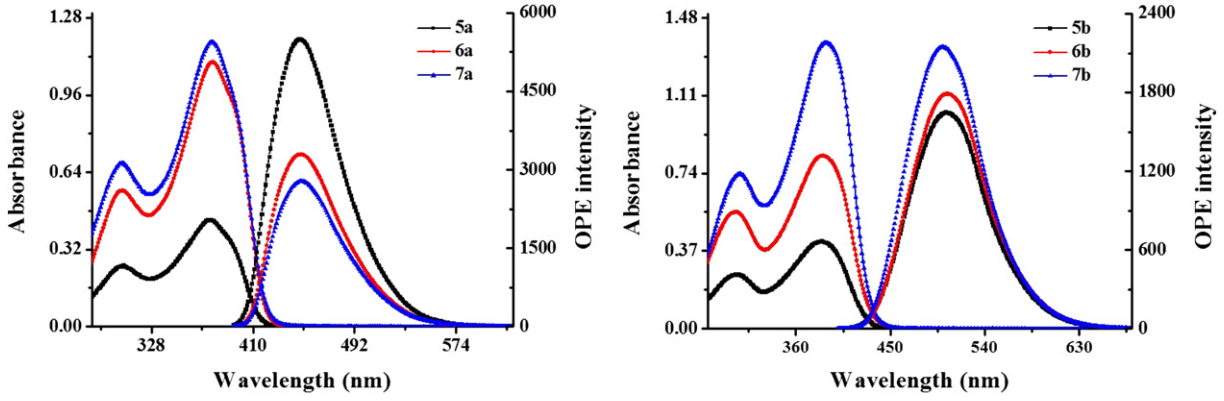

Fig. 2. OPA spectra (left) and OPEF spectra (right) of dyes **5a**–**7a** and **5b**–**7b** in DMF with a concentration of 1×10^{-5} mol L^{-1}.

3.2.3. The linear optical properties of different electron-donating group

As can be seen in Fig. 3, the OPA maxima and the OPEF maxima of dyes **5a**–**5b**, **6a**–**6b** and **7a**–**7b** in DMF all show obvious bathochromic shifts from a to b, respectively. They are all in agreement with the order of the extension of the π-systems: 4-ethoxy-*N*-(4-ethoxyphenyl)-*N*-phenylaniline > triphenylamine. Note that the maximum molar absorbance (ε_{max}) and the fluorescence quantum yield (Φ) of the dyes have to follow some rules. The maximum molar absorbance (ε_{max}) of dyes **5a**–**5b** and **6a**–**6b** show the same sequence of $\varepsilon_{max(\mathbf{5a})} > \varepsilon_{max(\mathbf{5b})}$ and $\varepsilon_{max(\mathbf{6a})} > \varepsilon_{max(\mathbf{6b})}$, while dyes **7a**–**7b** show a different sequence of $\varepsilon_{max(\mathbf{7b})} > \varepsilon_{max(\mathbf{7a})}$. While the fluorescence quantum yield (Φ) of dyes **5a**–**5b**, **6a**–**6b** and **7a**–**7b** all show the same sequence of $\Phi_{(\mathbf{5a})} > \Phi_{(\mathbf{5b})}$, $\Phi_{(\mathbf{6a})} > \Phi_{(\mathbf{6b})}$ and $\Phi_{(\mathbf{7a})} > \Phi_{(\mathbf{7b})}$. Interestingly, the Φ value of dyes **5b**–**7b** is depressed in comparison with dyes **5a**–**7a**, suggesting that although the flexible 4-ethoxy-*N*-(4-ethoxyphenyl)-*N*-phenylaniline chains function as solubilizing groups, it also enhances the nonradiative decay pathways. Therefore, we draw a conclusion that the dyes with triphenylamine as the donating end-groups appear to have high Φ and ε_{max} values compared with the dyes with 4-ethoxy-*N*-(4-ethoxyphenyl)-*N*-phenylaniline as the donating end-groups.

3.3. Two-photon properties

The two-photon excited fluorescence spectra (TPEF) of six dyes in DMF were recorded at their maximum excitation wavelength with a pulse duration of 140 fs under 800 mw (milliwatt). The 2PA excited fluorescence spectra (TPEF) data of dyes **5a**–**7a** and **5b**–**7b** are described in Table 1, which were measured in DMF ($c = 1 \times 10^{-3}$ mol L^{-1}). Representative TPEF spectra of dye **7b** are shown in Fig. 4a and b, while the others are included in the Supporting Information (Figs. S2 and S3).

Two-photon fluorescence spectra of dye **7b** in DMF pumped by femtosecond laser pulses at 800 mw at different excitation wavelengths are presented in Fig. 4a (others are found in Fig. S2). Fig. 4b shows 2PF spectra of dye **7b** under different pump intensities (others are found in Fig. S3), and the insets show logarithmic plots of the fluorescence integral versus pumped powers with a slope of 1.93 when the input laser power is increasing, suggesting a two-photon excitation mechanism. As no linear absorption was observed in the range from 500 nm to 2000 nm, so the emission excited by 790 nm laser wavelength can be attributed to the TPEF mechanism. As shown in Fig. 4c, all the six dyes display 2PA activity in the range of 720–880 nm in DMF.

It can be seen from Table 1 that the fluorescence peak wavelengths are evidently red-shifted by 23–42 nm by comparing with those of OPEF in DMF, which can be explained by the reabsorption effect. For one-photon induced emission measurements, we used dilute solutions (1×10^{-5} mol L^{-1}), thus the reabsorption of the fluorescence within the samples is negligible. In the case of two-photon excitation, concentrated solutions (1×10^{-3} mol L^{-1}) were used. Since the 790 nm laser beam can pass through the whole solution without linear depletion, the fluorescence emission is not only from the surface layer, but also from inside the solution sample. As a result, the reabsorption of the shorter wavelength fluorescence by the concentrated sample can no longer be neglected. The short wavelength side of the two-photon fluorescence was reabsorbed by the solution and red shifts of the fluorescence spectra were readily observed [17]. As shown in Fig. 5, the intensities of TPEF of dyes **5b**–**7b** exhibit the sequence of **5b** < **6b** << **7b**. These similarities between TPEF and OPEF indicate that both the emissions for a given dye are from the same excited state, though their initial Frank–Condon states may be different. The difference between TPEF and OPEF is mainly during the excitation process: two-photon absorption *vs* single-photon absorption.

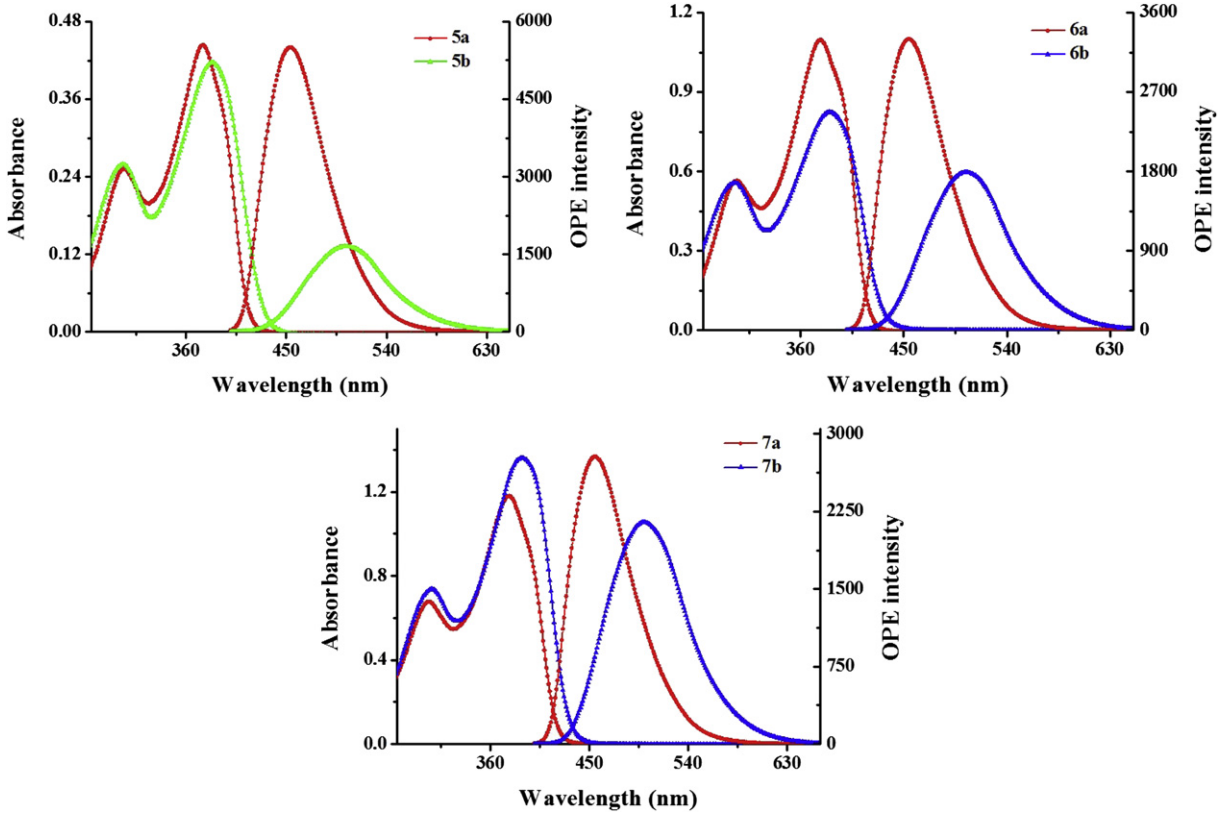

Fig. 3. OPA spectra (left) and OPEF spectra (right) of dyes **5a**–**5b**, **6a**–**6b** and **7a**–**7b** in DMF with a concentration of 1×10^{-5} mol L^{-1}.

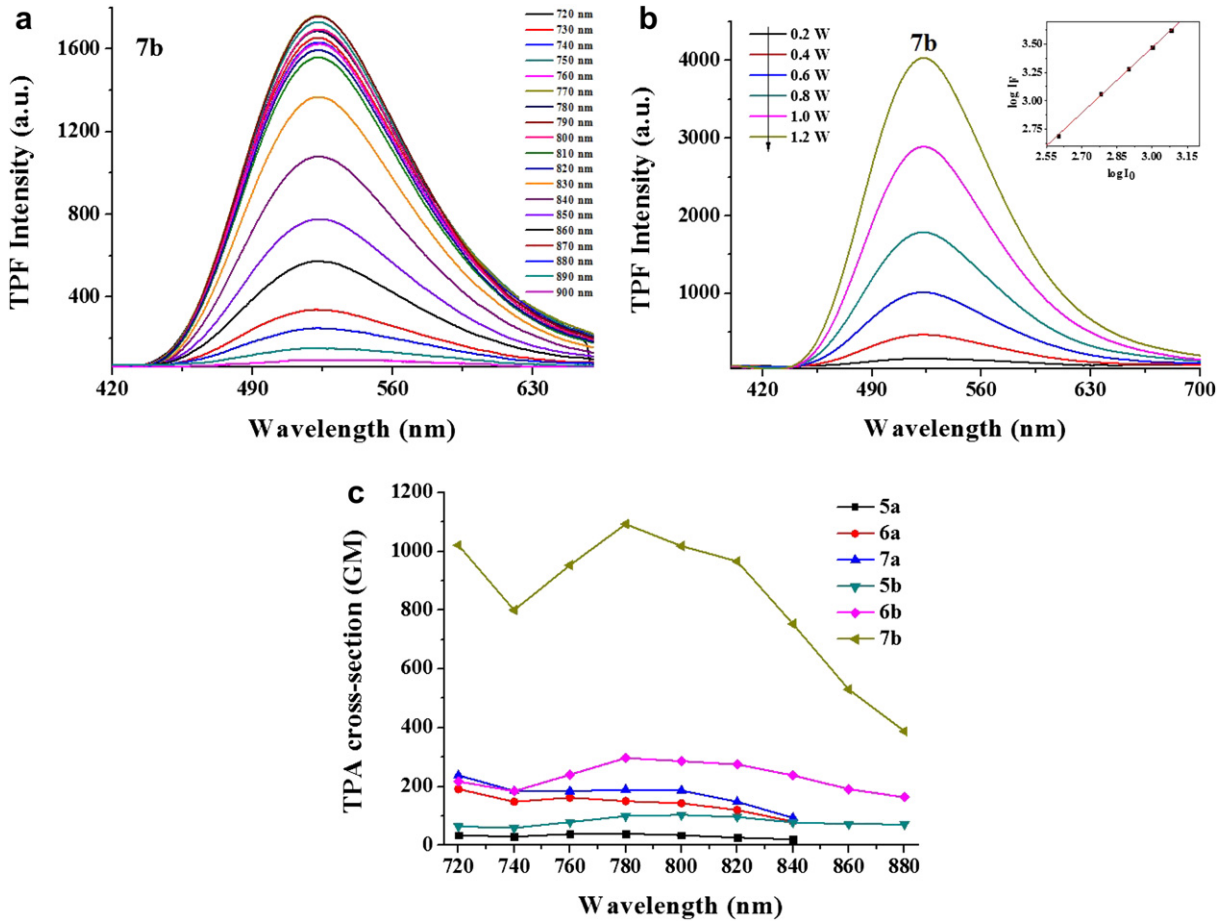

Fig. 4. (a) Two-photon fluorescence spectra of dye **7b** in DMF pumped by femtosecond laser pulses at 800 mw at different excitation wavelength. (b) 2PF spectra of dye **7b** in DMF under different pumped powers at 790 nm, insert contains the logarithmic plots of the fluorescence integral of chromophores versus different excitation intensities. (c) Two-photon absorption cross sections of dyes **5a**–**7a** and **5b**–**7b** in 720–880 nm regions.

As shown in Table 1 and Fig. 5, the 2PA cross section values (σ) increases obviously as the branch number increases in the series of dyes **5a**–**7a** and **5b**–**7b**. The reduced 2PA cross section σ/MW, which is defined as σ divided by the molecular weight, varies in a proportion of 1.0:2.6:2.4 for dyes **5a**–**7a** and 1.0:1.6:4.2 for dyes **5b**–**7b**, respectively. This means that the unit molecular weight enables enhanced 2PA cross section values as the branch number increases. This leads to the indication of some interactions between branches in the molecule, thus resulting in charge redistribution and extended delocalization. Consequently, the enhancement effect works in both linear and non-linear 2PA processes for dyes **5a**–**7a** and **5b**–**7b**. Note that the non-linear spectroscopic behavior of dye **6b** resembles that of dye **5b**, but does not resemble that of dye **7b**. It is different from dye **5a**–**7a** that dye **6a** resembles that of dye **7a**.

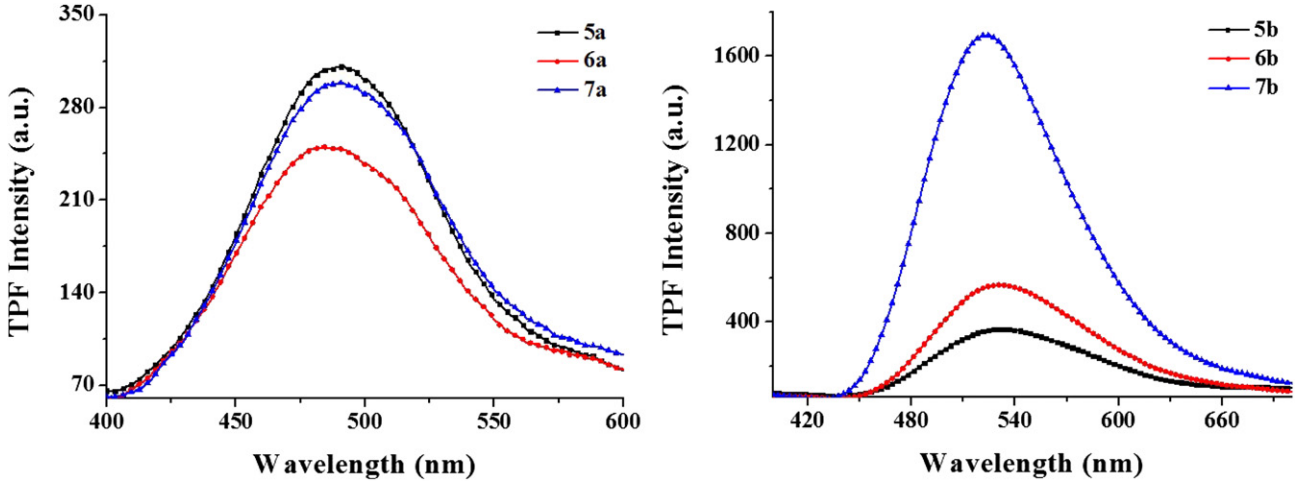

Fig. 5. The two-photon fluorescence spectra of dyes **5a**–**7a** and **5b**–**7b** in DMF ($c = 1 \times 10^{-3}$ mol L^{-1}).

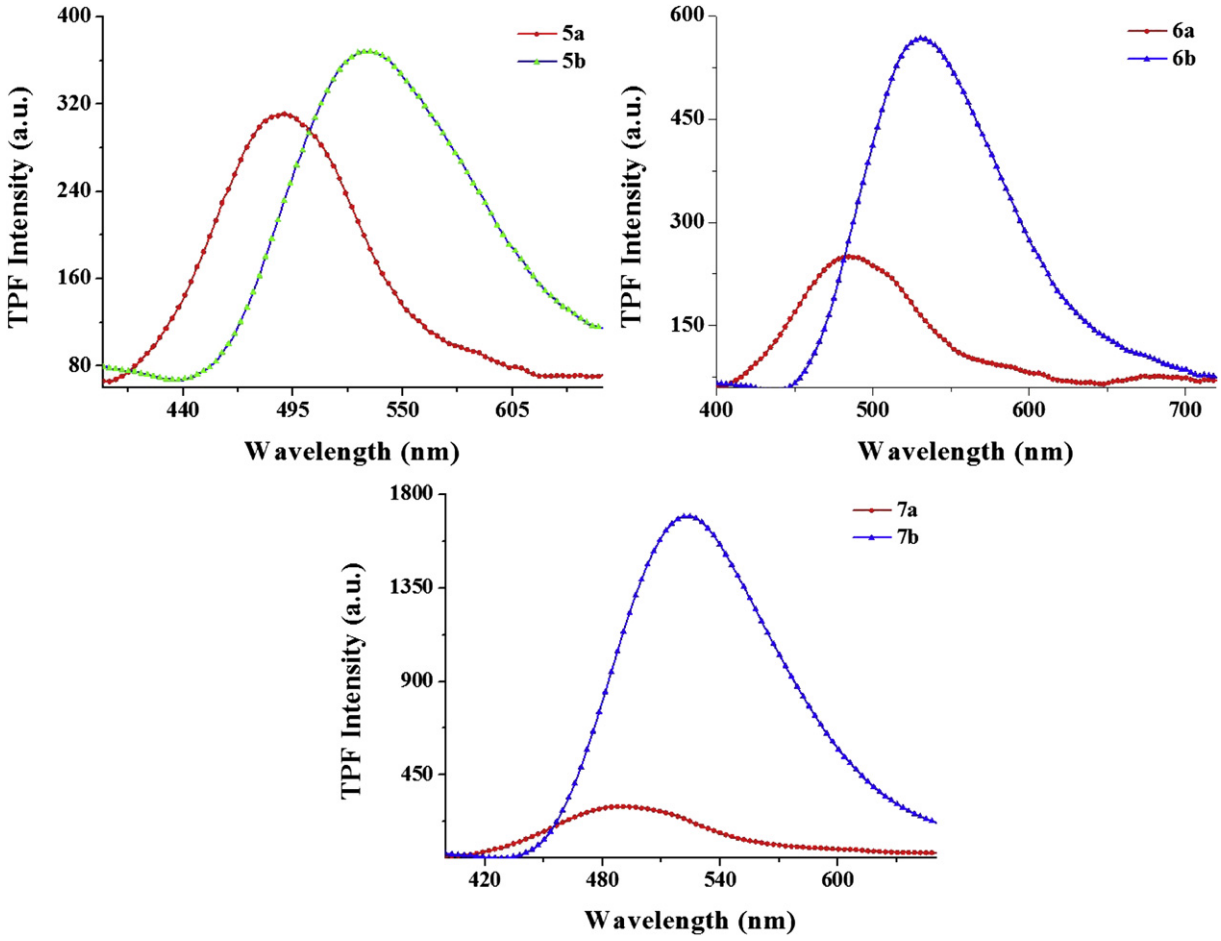

Fig. 6. The two-photon fluorescence spectra of dyes **5a**–**5b**, **6a**–**6b** and **7a**–**7b** in DMF ($c = 1 \times 10^{-3}$ mol L^{-1}).

As shown in Fig. 6, by comparing dye **5a** and dye **5b**, dye **6a** and dye **6b**, dye **7a** and dye **7b**, respectively, introducing an ethoxy terminal groups results in an obvious red-shift in two-photon fluorescence maxima and showing increased TPEF intensity from b to c. The possible reason is that the ethoxy group increases the electron-donating strength of the end group and also extends the conjugation length of the system. In addition, it was found that dye **7b** has a larger σ value of 1018 GM than the other five dyes because of the introduction of the ethoxy group.

According to Beljonne's exciton model [18], the extra enhancement in 2PA response for octupolar dyes can be achieved when the core allows significant electronic coupling between the individual branches. With respect to our system, a nitrogen atom as the linkage was adopted to combine 1, 3, 5-triazine core with substituents to accomplish a large 2PA cross section (1018 GM) which indicates that the lone pair electrons on the amino nitrogen atom of dye **7b** (also in **5b** and **6b**) may have delocalized onto the conjugated system of the molecule and this may increase intramolecular charge-transfer. Moreover, these well-conjugated structures allow sufficient electronic coupling between the branches, which has also been experimentally confirmed by the above-mentioned linear and non-linear photophysical data.

3.4. Cytotoxicity tests (MTT assay)

Considering their application in 2PF imaging, the MTT assay was performed to ascertain the cytotoxic effect of dyes **6a**–**7a**, **6b**–**7b** against MCF-7 cells over a 24 h period. Cytotoxicity is a potential side effect of dyes that must be controlled when dealing with living cells or tissues. Fig. 7 shows the cell viability for MCF-7 cells treated with dyes **6a**–**7a**, **6b**–**7b** at different concentrations for 24 h. The results clearly indicated that MCF-7 cells incubated with concentration of 1 μm of dye **7a** remained almost 100% viable after 24 h of feeding time, demonstrating the superior biocompatibility of the compound dye **7a**. This is also supported by live/dead co-staining studies. Besides, it was found that high concentration only leads to a gradual decrease of viable cells as shown in Fig. 7. As a result, cytotoxicity tests definitely indicate that the low-micromolar concentrations of dye **7a** would not give rise to obvious toxic effects on living cells over a period of 24 h, and dye **7a** is indeed has great potentials for further biological studies.

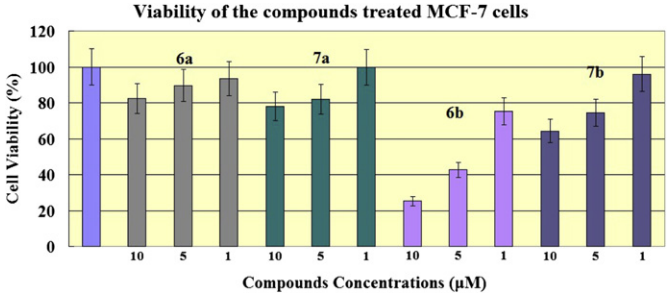

Fig. 7. MTT assay of MCF-7 cells treated with dyes **6a**–**7a**, **6b**–**7b** at different concentrations for 24 h.

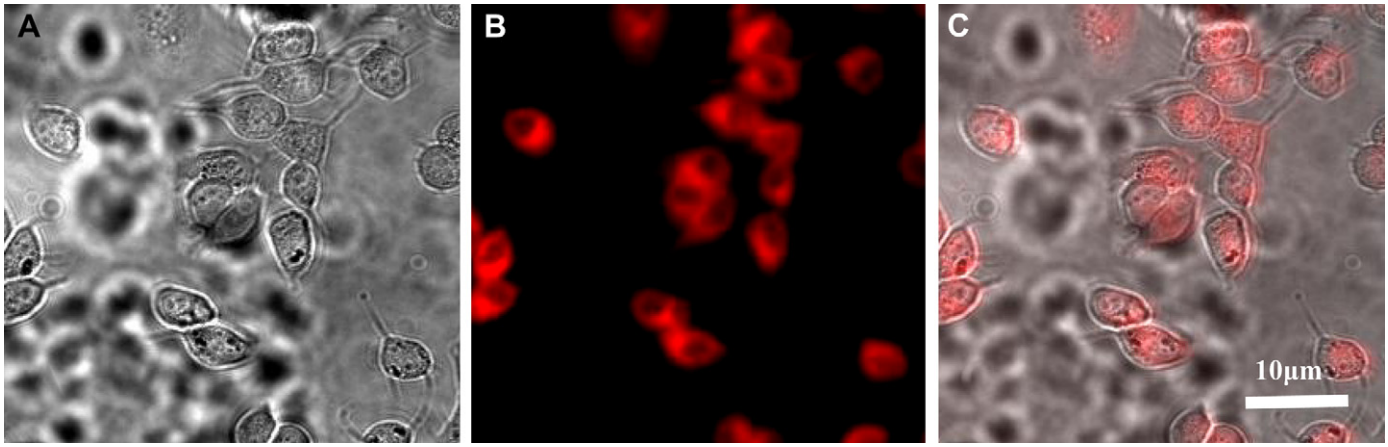

Fig. 8. (A) Bright-field image of the MCF-7 cells stained with dye **7a** (1 μm) for 2 h at 37 °C. (B) Two-photon fluorescence microscopy (2PFM) image of the same cells with excitation at 720–750 nm. (C) Merged image.

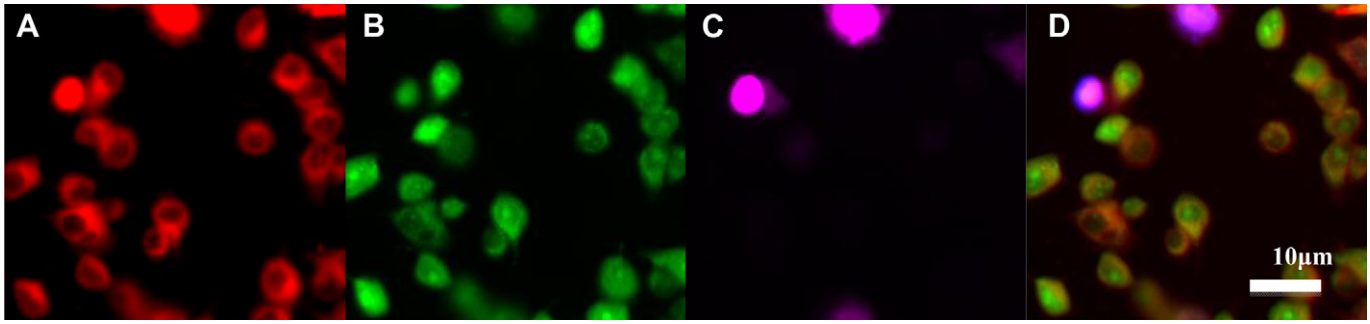

Fig. 9. (A) 2PFM image of the MCF-7 cells stained with dye **7a** (excitation at 720–750 nm). (B) Labeling of MCF-7 cells with SYTO-9® (λ_{ex} = 488 nm, λ_{em} = 500–530 nm) and (C) PI (λ_{ex} = 543 nm, λ_{em} = 560–580 nm) for 10 min after stained with dye **7a**. (D) Merged image.

3.5. *Two-photon microscopy bio-imaging application of dye **7a***

To evaluate the performance of dye **7a** in living cells, a two-photon fluorescence microscopy (2PFM) imaging, live/dead costaning was performed using 2 μM SYTO9® (live) and 10 μM PI (dead) and a cytotoxicity analysis were conducted. MCF-7 cells (human breast cancer cell line) were the testing candidates and were cultured and stained with dye **7a**. A bright-field image (Fig. 8A) of each cell was taken immediately prior to the 2PFM imaging. The 2PFM image and the merged image show that after 2 h incubation with MCF-7 cells (Fig. 8B,C), the complex went through the membrane and just localized uniformly in the cytoplasm. The intense fluorescence is mainly from dye **7a** internalized in the MCF-7 cell cytoplasm and the distribution in the nucleolus is significantly lower, suggesting that the cell cytoplasm can only be labeled by dye **7a**.

In order to observe the cell viability of the MCF-7 cells after stained with dye **7a**, costaining was performed using 2 μM SYTO-9® (λ_{ex} = 488 nm, λ_{em} = 500–530 nm) and 10 μM PI (λ_{ex} = 543 nm, λ_{em} = 560–580 nm) for 10 min after staining with dye **7a** in PBS (Fig. 9A). When SYTO-9® dye and propidium iodide (PI) are used in combination, intact cells are labeled green and cells with damaged membranes are labeled red. CLSM (Confocal Laser Scanning Microscope) images showed the appearance of both green (Fig. 9B) and red (Fig. 9C) cells, representing live and dead cells, respectively. Because SYTO-9® dye is able to penetrate all the cells and colour them green, the red cells represented dead cells which are permeable to PI as well, whose bound SYTO-9® stain was displaced by PI due to its high affinity for DNA [32], leaving the cells red. Most of the MCF-7 cells were mainly green, indicating a larger number of live cells (Fig. 9D) than dead cells. These results demonstrate the bio-imaging application of dye **7a** by labeling MCF-7 cells and also its low toxicity for living cells (also supported by MTT).

4. Conclusions

We have reported one-step syntheses of a series of multi-branched two-photon absorbing triazine dyes by changing the ratio of RNH_2 and 2, 4, 6-trichloro-1, 3, 5-triazine. The studies further demonstrated that having a σ-electron pair as bridge is an efficient way to transfer charge as well as a π bridge to induce a large 2PA cross section, and their 2PA cross section values (δ) increase with increasing electron-donating strength of the end-groups and branch number. Among the nine dyes, dye **7b** was found to exhibit a large 2PA across section values (1018 GM) as measured by the two-photon induced fluorescence methods, and low-micromolar concentrations of dye **7a** were tested showing no obvious toxic effect in imaging MCF-7 cells. Moreover, we also demonstrated that dye **7a** offers a potential application in two-photon fluorescence imaging due to its excellent biocompatibility and low toxicity. We believe that the design method and fabrication strategy are potentially applicable to the derivatization of analogous two-photon absorption dyes.

Acknowledgments

This work was supported by Program for New Century Excellent Talents in University (China), Doctoral Program Foundation of Ministry of Education of China (20113401110004), Science and Technological Fund of Anhui Province for Outstanding Youth (10040606Y22), National Natural Science Foundation of China

(21071001, 51142011 and 21101001), Natural Science Foundation of Education Committee of Anhui Province (KJ2012A024, KJ2010A030), the 211 Project of Anhui University, the Team for Scientific Innovation Foundation of Anhui Province (2006KJ007TD), Ministry of Education Funded Projects Focus on Returned Overseas Scholar, and Anhui University Student Innovative Experiment Plan (XJ103575023, KYXL201100337). Thank Lingxia Zheng of Department of Physcics and Materials Science of City University of Hong Kong for her help in writing the paper.

Appendix A. Supporting information

Supplementary data associated with this article can be found, in the online version, at doi:10.1016/j.dyepig.2012.03.017.

References

[1] Pawlicki M, Collins HA, Denning RG, Anderson HL. Two-photon absorption and the design of two-photon dyes. Angew Chem Int Ed 2009;48:3244–66.
[2] Terenziani F, Katan C, Badaeva E, Tretiak S, Blanchard-Desce M. Enhanced two-photon absorption of organic chromophores: theoretical and experimental assessments. Adv Mater 2008;20:4641–78.
[3] (a) Yao Sh, Ahn HY, Wang XH, Fu J, Stryland EWV, Hagan David, et al. Donor–acceptor–donor fluorene derivatives for two-photon fluorescence lysosomal imaging. J Org Chem 2010;75:3965–74;
(b) Andrade CD, Yanez CO, Rodriguez L, Belfield KD. A series of fluorene-based two-photon absorbing molecules: synthesis, linear and nonlinear characterization, and bioimaging. J Org Chem 2010;75:3975–82;
(c) Dvornikov AS, Walker EP, Rentzepis PM. Two-photon three-dimensional optical storage memory. J Phys Chem A 2009;113:13633–44;
(d) Tian H, Feng YL. Next step of photochromic switches? J Mater Chem 2008; 18:1617–22;
(e) Barsu C, Cheaib R, Chambert S, Queneau Y, Maury O, Cottet D, et al. Neutral push–pull chromophores for nonlinear optical imaging of cell membranes. Org Biomol Chem 2010;8:142–50;
(f) Lin TC, Haung YJ, Chen YF, Hu CL. Two-photon absorption and effective broadband optical power limiting properties of a multi-branched chromophore containing 2,3-diarylquinoxalinyl moieties as the electron-pulling units. Tetrahedron 2010;66:1375–82;
(g) LaFratta CN, Fourkas JT, Baldacchini T, Farrer RA. Multiphoton fabrication. Angew Chem Int Ed 2007;46:6238–58;
(h) Cumpston BH, Ananthavel SP, Barlow S, Dyer DL, Ehrlich JE, Erskine LL, et al. Two-photon polymerization initiators for three-dimensional optical data storage and microfabrication. Nature 1999;398:51–4.
[4] Zipfel WR, Williams RM, Webb WW. Nonlinear magic: multiphoton microscopy in the biosciences. Nat Biotechnol 2003;21:1369–77.
[5] Denk W, Strickler JH, Webb WW. Two-photon laser scanning fluorescence microscopy. Science 1990;248:73–6.
[6] (a) Hrobáriková V, Hrobárik P, Gajdoš P, Fitilis I, Fakis M, Persephonis P, et al. Benzothiazole-based fluorophores of donor-π-acceptor-π-donor type displaying high two-photon absorption. J Org Chem 2010;75:3053–68;
(b) Kim HM, Cho BR. Two-photon materials with large two-photon cross sections. Structure–property relationship. Chem Commun; 2009:153–64;
(c) Kamada K, Iwase Y, Sakai K, Kondo K, Ohta KJ. Cationic two-photon absorption chromophores with double- and triple-bond cores in symmetric/asymmetric arrangements. Phys Chem C 2009;113:11469–74.
[7] Fitilis I, Fakis M, Polyzos I, Giannetas V, Persephonis P, Vellis P, et al. A two-photon absorption study of fluorene and carbazole derivatives. The role of the central core and the solvent polarity. Chem Phys Lett 2007;447:300–4.
[8] (a) Chakrabarti S, Ruud K. Large two-photon absorption cross section: molecular tweezer as a new promising class of compounds for nonlinear optics. Phys Chem Chem Phys 2009;11:2592–6;
(b) Zein S, Delbecq F, Simon D. A TD-DFT investigation of two-photon absorption of fluorene derivatives. Phys Chem Chem Phys 2009;11:694–702;
(c) Nguyen KA, Day PN, Pachter R. Effects of conjugation in length and dimension on two-photon properties of fluorene-based chromophores. Theor Chem Acc 2008;120:167–75;
(d) Wang CK, Macak P, Luo Y, Ågren H. Effects of π centers and symmetry on two-photon absorption cross sections of organic chromophores. J Chem Phys 2001;114:9813.
[9] Rudberg E, Salek P, Helgaker T, Agren H. Calculations of two-photon charge-transfer excitations using Coulomb-attenuated density-functional theory. J Chem Phys 2005;123:184108.
[10] Reinhardt BA, Brott LL, Clarson SJ, Dillard AG, Bhatt JC, Kannan R, et al. Highly active two-photon dyes: design, synthesis, and characterization toward application. Chem Mater 1998;10:1863–74.
[11] Albota M, Beljonne D, Bredas JL, Ehrlich JE, Fu JY, Heikal AA, et al. Design of organic molecules with large two-photon absorption crosssections. Science 1998;281:1653–6.
[12] (a) McDonagh AM, Humphrey MG, Samoc M, Luther-Davies B. Organometallic complexes for nonlinear optics. 17.1 synthesis, third-order optical nonlinearities, and two-photon absorption cross section of an alkynylruthenium dendrimer. Organometallics 1999;18:5195–7;
(b) Spangler CW. Recent development in the design of organic materials for optical power limiting. J Mater Chem 1999;9:2013–20.
[13] Cho BR, Son KH, Lee SH, Song YS, Lee YK, Jeon SJ, et al. Two photon absorption properties of 1,3,5-tricyano-2,4,6-tris(styryl)benzene derivatives. J Am Chem Soc 2001;123:10039–45.
[14] Kim HM, Seo MS, Jeon SJ, Cho BR. Two-photon absorption properties of hexa-substituted benzene derivatives. Comparison between dipolar and octupolar molecules. Chem Commun 2009;47:7422–4.
[15] Porrès L, Mongin O, Katan C, Charlot M, Pons T, Mertz J, et al. Enhanced two-photon absorption with novel octupolar propeller-shaped fluorophores derived from triphenylamine. Org Lett 2004;6:47–50.
[16] Collings JC, Poon SY, Le DC, Charlot M, Katan C, Palsson LO, et al. The synthesis and one- and two-photon optical properties of dipolar, quadrupolar and octupolar donor–acceptor molecules containing dimesitylboryl groups. Chem Eur J 2009;15:198–208.
[17] Xu F, Wang ZW, Gong QH. Synthesis, characterization, and optical properties of two-photon-absorbing octupolar molecule with an s-triazine core. Opt Mater 2007;29:723–7.
[18] Beljonne D, Wenseleers W, Zojer E, Shuai ZG, Vogel H, Pond SJK, et al. Role of dimensionality on the two-photon absorption response of conjugated molecules: the case of octupolar compounds. Adv Funct Mater 2002;12: 631–41.
[19] Jiang YH, Wang YC, Hua JL, Tang J, Li B, Qian SX, et al. Multibranched triarylamine end-capped triazines with aggregation-induced emission and large two-photon absorption cross-sections. Chem Commun 2010;46:4689–91.
[20] Jiang YH, Wang YC, Wang B, Yang JB, He NN, Qian ShX, et al. Synthesis, two-photon absorption and optical limiting properties of multi-branched styryl derivatives based on 1,3,5-triazine. Chem Asian J 2011;6:157–65.
[21] (a) Murase T, Fujita M. Highly blue luminescent triazine–amine conjugated oligomers. J Org Chem 2005;70:9269–78;
(b) El-Sedik M, Almonasy N, Nepraš M, Bureš F, Dvořák M, Michl M. Synthesis, absorption and fluorescence properties of N-triazinyl derivatives of 2-aminoanthracene. Dyes Pigm 2012;92:1126–31;
(c) Nepraš M, Almonasy N, Michl M, Dvořák M, Fidler V. Electronic structure, spectra and photophysical properties of N-triazinylderivatives of 1-aminopyrene. Semi-empirical theoretical study. Dyes Pigm 2012;92:1331–6.
[22] Yan YX, Fan HH, Guo YH, Lam CK, Huang H, Sun YH, et al. Synthesis and two-photon absorption property of new π-conjugated dendritic fluorophores containing styrylpyridyl moieties. Mater Chem Phys 2007;101:329–35.
[23] (a) Fink R, Frenz C, Thelakkat M, Schmidt HW. Synthesis and characterization of aromatic poly(1,3,5-triazine–ether)s for electroluminescent devices. Macromolecules 1997;30:8177–81;
(b) Inomata H, Goushi K, Masuko T, Konno T, Imai T, Sasabe H, et al. High-efficiency organic electrophosphorescent diodes using 1,3,5-triazine electron transport materials. Chem Mater 2004;16:1285–91;
(c) Zhong H, Xu E, Zeng D, Du J, Sun J, Ren S, et al. New optoelectronic materials based on bitriazines: synthesis and properties. Org Lett 2008;10: 709–12;
(d) Ren S, Fang Q, Yu F, Bu D. Synthesis and optical and electrochemical properties of new π-conjugated 1,3,5-triazine-containing polymers. J Polym Sci A Polym Chem 2005;43:6554–61.
[24] (a) Kannan R, He GS, Lin TC, Prasad PN, Vaia RA, Tan LS. Toward highly active two-photon absorbing liquids. Synthesis and characterization of 1,3,5-Triazine-Based octupolar molecules. Chem Mater 2004;16:185–94;
(b) Meng F, Li B, Qian S, Chen K, Tian H. Enhanced two-photon properties of tri-branched styryl derivatives based on 1,3,5-triazine. Chem Lett 2004; 33:470;
(c) Li B, Tong R, Zhu R, Meng F, Tian H, Qian S. The ultrafast dynamics and nonlinear optical properties of tribranched styryl derivatives based on 1,3,5-triazine. J Phys Chem B 2005;109:10705–10;
(d) Cui YZ, Fang Q, Xue G, Xu GB, Yin L, Yu WT. Cooperative enhancement of two-photon absorption of multibranched compounds with vinylenes attaching to the s-triazine core. Chem Lett 2005;34:644.
[25] (a) Ning ZJ, Tian H. Triarylamine: a promising core unit for efficient photovoltaic materials. Chem Commun; 2009:5483–95;
(b) Chen CY, Pootrakulchote N, Wu SJ, Wang M, Li JY, Tsai JH, et al. New ruthenium sensitizer with carbazole antennas for efficient and stable thin-film dye-sensitized solar cells. J Phys Chem C 2009;113:20752–7;
(c) Zhang XH, Wang ZS, Cui Y, Koumura N, Furube A, Hara K. Organic sensitizers based on hexylthiophene-functionalized indolo[3,2-b]carbazole for efficient dye-sensitized solar cells. J Phys Chem C 2009;113:13409–15;
(d) Hrobárik P, Sigmundová I, Zahradník P, Kasák P, Arion V, Franz E, et al. Molecular engineering of benzothiazolium salts with large quadratic hyperpolarizabilities: can auxiliary electron-withdrawing groups enhance nonlinear optical responses? J Phys Chem C 2010;114:22289–302;
(e) Moylan CR, Twieg RJ, Lee VY, Swanson SA, Betterton KM, Miller RD. Nonlinear optical chromophores with large hyperpolarizabilities and enhanced thermal stabilities. J Am Chem Soc 1993;115:12599–600;
(f) Whitaker CM, Patterson EV, Kott KL, McMahon RJ. Nitrogen and oxygen donors in nonlinear optical materials: effects of alkyl vs phenyl substitution on the molecular hyperpolarizability. J Am Chem Soc 1996;118:9966–73.

[26] Demas JN, Crosby GA. Measurement of photoluminescence quantum yields. Review J Phys Chem 1971;75:991–1024.
[27] Gray TG, Rudzinski CM, Meyer EE, Holm RH, Nocera DG. Spectroscopic and photophysical properties of hexanuclear rhenium(III) chalcogenide clusters. J Am Chem Soc 2003;125:4755–70.
[28] Lee SK, Yang WJ, Choi JJ, Kim CH, Jeon SJ, Cho BR. 2,6-Bis[4-(p-dihexylaminostyryl)styryl]anthracene derivatives with large two-photon cross sections. Org Lett 2005;7:323–6.
[29] Xu C, Webb WW. Measurement of two-photon excitation cross sections of molecular fluorophores with data from 690 to 1050 nm. J Opt Soc Am B 1996; 13:481–91.
[30] Whittall IR, Humphrey MG. Organometallic complexes for nonlinear optics. 3.1 molecular quadratic hyperpolarizabilities of ene-, imine-, and azo-linked ruthenium σ-acetylides: X-ray Crystal structure of Ru((E)-4,4′-C≡CC_6H_4CH=$CHC_6H_4NO_2$)$(PPh_3)_2(\eta$-$C_5H_5)$. Organometallics 1996;15:1935–41.
[31] Wang XM, Zhou YF, Yu WT, Wang Ch, Fang Q, Jiang MH, et al. Two-photon pumped lasing stilbene-type chromophores containing various terminal donor groups: relationship between lasing efficiency and intramolecular charge transfer. J Mater Chem 2000;10:2698–703.
[32] Bunthof CJ, Bloemen K, Breeuwer P, Rombouts FM, Abee T. Flow cytometric assessment of viability of lactic acid bacteria. Appl Environ Microbiol 2001;67: 2326–35.